



HAL
open science

Fundamental Mechanisms Behind the Reverse Characteristic of Cu(In,Ga)Se₂ Solar Cells

Klaas Bakker, Suzanne Assen, Alix Rasia, Nicolas Barreau, Arthur Weeber,
Mirjam Theelen

► **To cite this version:**

Klaas Bakker, Suzanne Assen, Alix Rasia, Nicolas Barreau, Arthur Weeber, et al.. Fundamental Mechanisms Behind the Reverse Characteristic of Cu(In,Ga)Se₂ Solar Cells. IEEE Journal of Photovoltaics, 2022, 12 (6), pp.1412 - 1417. 10.1109/JPHOTOV.2022.3196827 . hal-03791816

HAL Id: hal-03791816

<https://hal.science/hal-03791816v1>

Submitted on 29 Mar 2023

HAL is a multi-disciplinary open access archive for the deposit and dissemination of scientific research documents, whether they are published or not. The documents may come from teaching and research institutions in France or abroad, or from public or private research centers.

L'archive ouverte pluridisciplinaire **HAL**, est destinée au dépôt et à la diffusion de documents scientifiques de niveau recherche, publiés ou non, émanant des établissements d'enseignement et de recherche français ou étrangers, des laboratoires publics ou privés.

Fundamental Mechanisms Behind the Reverse Characteristic of Cu(In,Ga)Se₂ Solar Cells

Klaas Bakker, Suzanne Assen, Alix Rasia, Nicolas Barreau, Arthur Weeber, and Mirjam Theelen

Abstract—Partial shading of PV modules can lead to degradation of the shaded cells. The degradation originates from a reverse bias voltage over the shaded cells. In order to mitigate reverse bias damage in Cu(In,Ga)Se₂ (CIGS) modules a good understanding of the fundamental mechanisms governing the reverse characteristic is required. In this study a model is introduced that describes this behavior for CIGS cells. In this model the low and non-Ohmic leakage current is accounted for by the space charge limited current component. A sharp increase in current that is typically observed in the CIGS reverse characteristics can be described by Fowler - Nordheim tunneling. This model has been validated against measurements performed at different temperatures and illumination intensities, and is able to describe the dependencies of the reverse bias behavior on both temperature and illumination.

Index Terms—CIGS, reverse bias, partial shading, thin-film PV

I. INTRODUCTION

SOLAR cells in partial shaded PV modules can be subjected to reverse bias voltages. In Cu(In,Ga)Se₂ (CIGS) solar cells reverse bias voltages can lead to reversed bias induced defects, also known as wormlike defects [1]. Exposure to reverse bias can in general be mitigated by the inclusion of bypass diodes. However, most commercial CIGS modules are of the monolithic interconnected type where it is difficult to integrate bypass diodes to protect individual cells due to the layout of the module [2], [3]. Therefore, several authors have suggested to use the CIGS solar cell itself as a bypass diode [4]–[6]. This would be possible because the current density versus voltage (JV) characteristic at negative voltages shows a increase in current like a Zener or avalanche diode. This sharp increase resembles a transition between an isolating and conducting nature. The voltage at which this transition occurs, the transition voltage, strongly depends on illumination conditions [6]–[11].

This paragraph of the first footnote will contain the date on which you submitted your paper for review. This work is supported by ‘Netherlands Enterprise Agency’ (RVO) and the Dutch TopTeam Energy via the projects: ‘Building Integrated PhotoVoltaic Panels on Demand - in The Netherlands’ with grant number TEID215005 and ‘Performance and Electroluminescence Analysis on Reliability and Lifetime of Thin-Film Photovoltaics’ with grant number TEUE116203. Furthermore, the Early Research Program ‘Sustainability & Reliability for solar and other (opto-)electronic thin-film devices’ from TNO is acknowledged for funding.

K. Bakker is with the Photovoltaic Materials and Devices Group, Delft University of Technology, 2628 CD Delft, The Netherlands, and also with TNO

This is partly due to the increased photo-conductivity in the buffer layer as the color of illumination is an important parameter [7]–[9]. Low wavelength (blue) light, which is absorbed in the buffer layer, shifts the transition voltage to less negative voltages. This in contrast to high wavelength (red) light, for which the buffer is transparent. Cells illuminated with red light show similar behavior in a reverse bias scan as cells in the dark. Other parameters shown to have a large influence on the reverse characteristic are temperature [8], [9], buffer layer properties [8], [12], [13], and sodium concentration [9], [14].

Discussion exists in literature on the mechanism behind the transition. In the earlier publications [8], [9] the mechanism behind the transition in the dark is described to be the result of impact ionization (avalanche effect), tunneling (Zener effect) or a combination of avalanche and tunneling that may be assisted by defects or metastable interface charges [7]. Understanding the mechanisms and transferring them into a model is essential for predicting the behavior of PV modules under partial shaded conditions [10], [15], and in the end mitigate the impact.

The first model that was able to simulate the reverse characteristic was introduced by Sun *et al.* [11]. This model was used to simulate the electro-thermal behavior of monolithically interconnected CIGS modules under partial shading [10], [11]. This model explained the reverse characteristic by using tunneling through defects (Poole - Frenkel mechanism) and was also able to explain the light dependency by introducing a pre-exponential factor. Szaniawski *et al.* [13] introduced a model based on fitting of the reverse characteristic of several CIGS cells. The model of Szaniawski *et al.* uses a combination of the Poole - Frenkel mechanism and the Fowler - Nordheim mechanism. The Fowler - Nordheim mechanism describes tunneling through a triangular energy barrier, which Szaniawski *et al.* assumed to be the buffer layer. In this model Fowler - Nordheim tunneling is the dominant mechanism and the Poole - Frenkel mechanism is used to explain the discrepancy at lower currents. However, this model is not able to explain the light dependency of the reverse characteristic.

partner in Solliance, 5656 AE Eindhoven, The Netherlands (e-mail: klaas.bakker@tno.nl).

S. Assen, A. Rasia and M. Theelen are with TNO partner in Solliance, 5656 AE Eindhoven, The Netherlands (e-mail: mirjam.theelen@tno.nl).

N. Barreau is with the Institut des Matériaux Jean Rouxel, Université de Nantes, 44322 Nantes, France (e-mail: nicolas.barreau@univ-nantes.fr).

A. Weeber is with the Photovoltaic Materials and Devices Group, Delft University of Technology, 2628 CD Delft, The Netherlands, and also with TNO Energy Transition, Westerdinweg 3, 1755 LE, Petten, The Netherlands (e-mail: a.w.weeber@tudelft.nl).

In this study the reverse characteristic at different temperatures and illumination conditions were measured. Based on these measurements we propose a model that explains both the temperature and illumination dependence of the reverse characteristic of CIGS cells.

II. EXPERIMENTAL DETAILS

The single cell, described in this study, survived all measurement sequences, and has been used in previous studies [16], [17] (sample I-2 in [17]). The measurement sequence for this cell was:

- 1) Initial JV scan, 20 months after fabrication
- 2) Variable irradiance measurements, 12 days after initial JV
- 3) Dark temperature scan, 158 days after initial JV scan
- 4) Illuminated temperature scan, 168 days after initial JV

The cell was stored in an inert environment in between measurements. The design of this cell resembles a cell in a monolithically interconnected module and therefore has no grid. To reduce series resistance losses a thicker transparent conductive oxide (TCO) is used, that makes the cell more robust against reverse bias damage [12]. Downside of this design is that the efficiency is slightly lower. The layer stack is made out of: 1 mm soda-lime glass (SLG), 500 nm DC-sputtered molybdenum (Mo), 2 μm co-evaporated CIGS, 50 nm chemical bath deposited cadmium sulfide (CdS), 65 nm DC sputtered intrinsic zinc oxide (i-ZnO), 1 μm DC sputtered aluminum doped zinc oxide (AZO) and 60 nm thermally evaporated gold (Au) contacts to the sides [17].

An initial reverse JV scan was performed in a dark enclosure using a Keithley 2400, ranging from +0.7 V till -10.0 V with the compliance set to 100 mA (294 mA/cm²) and a scan speed of 100 mV/sec. The JV measurements for variable irradiance measurements (VIR) and temperature scans were carried out with a Neonsee class AAA AM1.5G solar simulator type IV-SS-30V. The wide range irradiance control option of this simulator allows for attenuation of the irradiance while maintaining AM1.5G spectrum and was used to control the irradiance for both VIR and temperature scans. For the temperature scans the sample was mounted in a Linkam THMS600 stage. Scan settings for VIR; from +0.7 V till -9.3 V, compliance of 50 mA (147 mA/cm²) and a scan speed of 147 mV/sec. The JV sweeps for the temperature scans were performed with a scan speed of 273 mV/sec from +0.7 V till -6 V and a current limit of 17.5 mA (51.5 mA/cm²) and 25 mA (73.5 mA/cm²) for the dark and illuminated measurements respectively.

III. RESULTS AND DISCUSSION

A. Components of the model

Szaniawski *et al.* [13] proposed a model based on the work of Sun *et al.* [11] in which the Fowler - Nordheim mechanism is responsible for the large increase in current after the transition. Furthermore, they also observed an increase in current already before the transition. Szaniawski *et al.* [13] explained this by the Poole - Frenkel model, where Sun *et al.* [11] used the space charge limited current (SCLC) [18], [19] to

explain this non-ohmic current.

The model used in this study is using the Fowler - Nordheim (FN) mechanism as the dominant mechanism. Furthermore, the Poole - Frenkel (PF) and SCLC mechanisms are used to explain the non-Ohmic behavior before the transition that can not be explained by the Fowler - Nordheim mechanism. The equations for the current density as a results of the Fowler - Nordheim (J_{FN}) and Poole - Frenkel (J_{PF}) mechanisms are based on Szaniawski *et al.* [13] and are given in (1) and (2), respectively.

$$J_{FN} = C_{FN} \frac{q^3 E^2}{8\pi\Phi_{FN}} \frac{m^*}{m_e} \exp\left[-\frac{8\pi\sqrt{2m^*\Phi_{FN}^3}}{3qhE}\right] \quad (1)$$

$$J_{PF} = q\mu N_C E \exp\left[-\frac{q\left(\Phi_{PF} - \sqrt{\frac{qE}{\pi\epsilon_i\epsilon_0}}\right)}{k_B T}\right] \quad (2)$$

A list of all constants and variables used can be found in Table I.

TABLE I
CONSTANTS AND VARIABLES USED IN SIMULATIONS

Parameter	Definition	Value and Unit
C_{FN}	Correction factor for Fowler - Nordheim	-
q	Elementary charge	1.602×10^{-19} C
E	Electric field	V/m
m^*	Effective mass of electron in CIGS	9.109×10^{-32} kg
m_e	Mass of electron	9.109×10^{-31} kg
Φ_{FN}	Fowler - Nordheim barrier	eV
h	Planck constant	6.626×10^{-34} Js
μ	Electron mobility	1×10^{-2} m ² /(Vs)
N_C	Density of states in the conduction band	2×10^{24} m ⁻³
Φ_{PF}	Poole - Frenkel barrier	V
ϵ_i	Dielectric constant of CIGS	13
ϵ_0	Permittivity of free space	8.854×10^{-12} F/m
k_B	Boltzmann constant	1.381×10^{-23} J/K
T	Temperature	K
k	Coefficient of SCLC component	A/V ^m
m	SCLC power factor	-
V^*	Voltage after series resistance losses	V
D	Thickness of buffer layer	m
V	Applied voltage	V
J	Current density through cell	A/m ²
J_{photo}	Light generated current density	A/m ²
J_{FN}	Fowler - Nordheim current density	A/m ²
J_{PF}	Poole - Frenkel current density	A/m ²
J_{SCLC}	Space charge limited current density	A/m ²
J_{shunt}	Shunt resistance current density	A/m ²
R_s	Series resistance	Ωm^2
R_{shunt}	Shunt resistance	Ωm^2

In (1) and (2) E is the electric field over the buffer layer, as described by Szaniawski *et al.* [13]:

$$E = \frac{V^*}{d} \quad (3)$$

Both mechanisms describe electron transport through the buffer layer in the presence of an electric field.

The FN equation (1) describes tunneling through a triangular barrier, the only material related parameter in this equation is the effective mass of the electron. The rest of the parameters are all physical constants. In order to incorporate changes in the device due to dependencies of light and temperature a pre-exponential factor C_{FN} was introduced.

The PF formula (2) describes trap assisted electron transport,

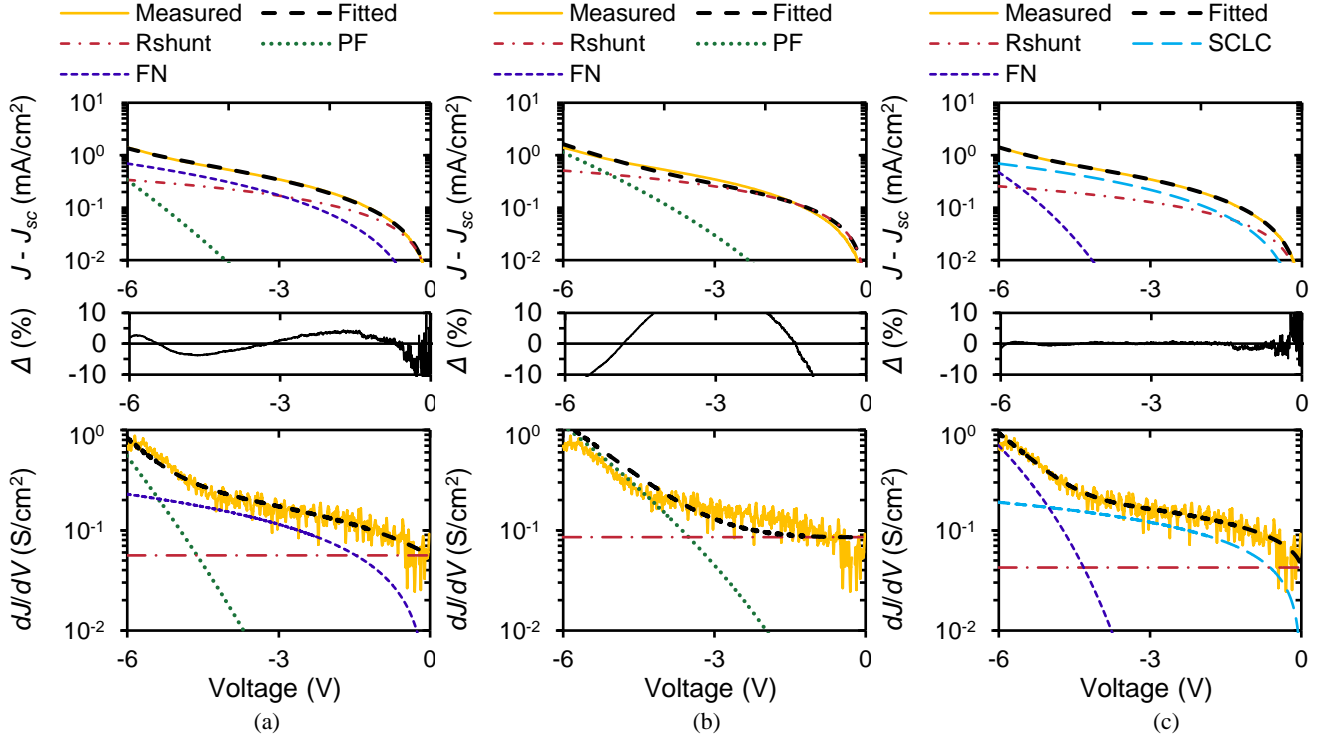


Fig. 1: Dark reverse characteristic of one CIGS solar cell measured at 267K. The same measurement is fitted with different pre-breakdown mechanisms. In (a), (b), and (c) the x-axis in all graphs is voltage, the top graph is the JV graph on a semi-log scale, the middle graph is the difference (Δ) between measured and fitted data, and the bottom graph shows the derivative of the top graph. In (a) and (b) a combination of J_{FN} , J_{PF} , and J_{shunt} was used. In (a) the fitting routine was started with a low value for Φ_{PF} (0.5V) while in (b) it was started with a high Poole - Frenkel barrier (1.2V). For (c) the combination J_{FN} , J_{SCLC} , and J_{shunt} was used for the fitting.

from the formula it can be seen that it depends on material parameters and temperature. The material parameters being conduction ($q\mu N_C$) and the dielectric constant (ϵ_i). For this study the conductivity has been kept constant, and no pre-exponential factor has been used. This would not directly change the outcome of the fit but would have an impact on the voltage barrier Φ_{PF} , according to the rules for exponents ($\exp^a \times \exp^b = \exp^{(a+b)}$).

For all fittings the CIGS material parameters from Szaniawski *et al.* [13] have been taken over. Since E is assumed to be the field over the buffer layer, it could be argued that material parameters for CdS would be more appropriate. However, we found a constant difference in Fowler - Nordheim parameters ($35.8 \pm 0.4\%$ for Φ_{FN} and $-45.4 \pm 1.5\%$ for C_{FN}) when CdS parameters were used. Furthermore, the chi-square, used to determine the goodness of the fit, remained unchanged, and trends remain the same. Because of the constant difference we can conclude that FN tunneling is the main mechanism responsible for the reverse bias behavior. The exact nature of the tunneling barrier will be determined by material properties of the complex stack between the AZO and the quasi-neutral bulk CIGS material. Therefore, the exact parameters are difficult to determine, and need further investigation.

For all equations V^* is the voltage minus the series resistance losses and is:

$$V^* = |V| - (|J|R_s) \quad (4)$$

Note that for the fitting the absolute values of voltage and current density were used.

Equations (5) and (6) give the current densities as results of the SCLC (J_{SCLC}) and shunt resistance (J_{shunt}), respectively.

$$J_{SCLC} = k(V^*)^m \quad (5)$$

$$J_{shunt} = \frac{V^*}{R_{shunt}} \quad (6)$$

The total current density through the cell at reverse bias is the sum of the contributions and given in (7). Where J_{photo} is the light generated current.

$$J = -(J_{photo} + J_{FN} + J_{PF} + J_{SCLC} + J_{shunt}) \quad (7)$$

Each of the individual contributions can be omitted, or set to zero, for example J_{photo} is zero for dark measurements, and is used as a free fitting parameter for the illuminated measurements.

B. Pre-transition mechanism

The pre-transition mechanism is the mechanism responsible for the small non-ohmic leakage current observed at low absolute voltages. Fig. 1 shows the measurements and fits to different combinations of components for a dark reverse characteristic at 267 K. Cooling the cell attenuates the mechanism responsible for the transition [8], [9]. Therefore, cooling allows for closer inspection of the small non-ohmic leakage current. Fig. 1 (a) and (b) both show fits with J_{SCLC} set to zero in (7). As starting value for the fit 0.5 and 1.2 V where used for Φ_{PF} for (a) and (b) respectively. The results displayed in Fig. 1 (a) and (b) show that the PF mechanism is not able to describe the small non-Ohmic pre-breakdown current. The outcome is strongly depending on the starting conditions. Even when the FN contribution is fixed, the PF mechanism is at lower temperatures not able to describe the pre-breakdown current accurately. Adding a pre-exponential correction factor as described by Sun *et al.* [11] does not alter the shape of the curve.

Furthermore, the numerical fitting procedure with a combination of PF and FN is not robust as the outcome strongly depends on the initial value of the parameters. In this case the additional freedom of two variable parameters forces the FN contribution either to zero (Fig. 1 (b)) or to contribute to the pre-breakdown current (Fig. 1 (a)). Fig. 1 (c) shows the results for fits with a combination of J_{FN} , J_{SCLC} , and J_{shunt} . As can be seen the SCLC fits the pre-transition current almost perfectly. This implies that in the dark the SCLC is the superior mechanism at all temperatures. In the next sections all fits will be performed with a combination of J_{SCLC} , and J_{shunt} for the pre-transition current and J_{FN} as the main transition current.

C. High injection, parameter drift, and series resistance

In Fig. 2 the results of two consecutive measurements are shown. The intention of these measurements was the creation of wormlike defects [16], [17], for which the sweep speed was set to a relatively slow 100 mV/sec and the current limit was set to a very high 294 mA/cm². Furthermore, the measurement was not aborted when the current limit was reached and the maximum current was injected into the cell till the end of the sweep. Two different features can be seen in Fig. 2. Firstly the reduced voltage at high currents and secondly the non-reproducible behavior.

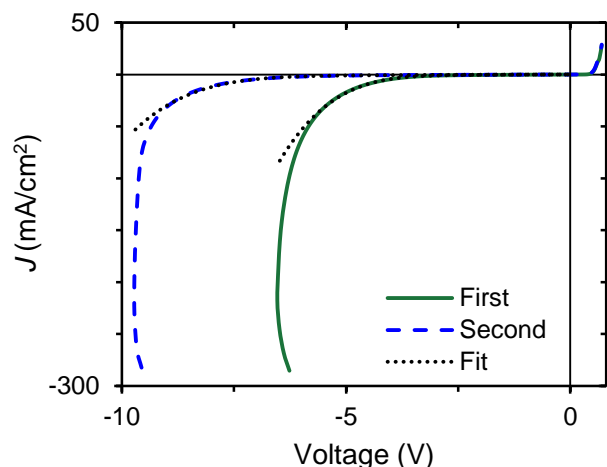


Fig. 2: Dark JV characteristics of two consecutive measurements. The first measurement is displayed as a green solid line, the second as a blue dashed line. For both measurements the fit results are represented in black dotted lines.

At high current densities the voltage over the cell is getting less negative, almost as if there was a negative series resistance. This behavior shows that the power dissipated by the cell during the measurement is causing the cell to heat up and alter the reverse characteristic during the measurement. For example the power ($V \cdot J$) dissipated at 50 mA/cm² is 312 and 470 mW/cm² for the first and second measurement respectively. At higher temperatures the transition shifts to less negative voltages. In the fitting this behavior is taken into account by fitting $J-J_{sc}$ up to 50 mA/cm² and by setting the series resistance to 0 $\Omega \cdot \text{cm}^2$.

Furthermore, there is a large discrepancy between the first and second measurement. Similar changes in the reverse characteristic caused by consecutive measurements have also been reported for CdS containing cells by Szaniawski *et al.*

[13]. Also, it has been observed that temperature and light soaking have an influence on the reverse characteristic [7].

In forward bias changes in the JV curves as a result of illumination and temperature have been observed [20]. These changes results in parameter drifts of mostly the open-circuit voltage (V_{oc}) and fill factor (FF), and are often called metastability. In order to avoid confusion the term parameter drift is used in this study to describe the changes in reverse bias behavior. The principles behind the parameter drift are not yet understood and is something to keep in mind when studying the reverse characteristic.

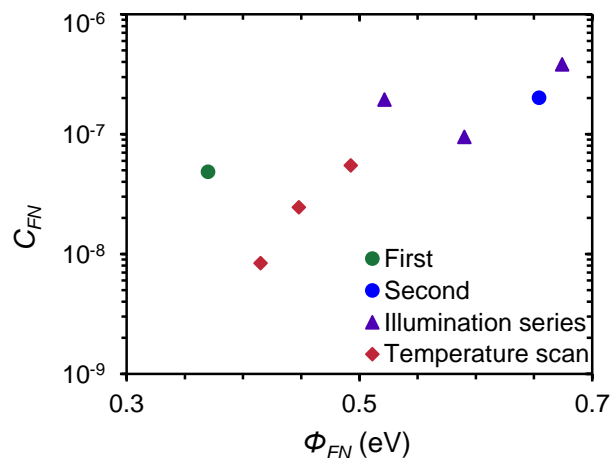


Fig. 3: Fit results of comparable dark measurements, with on the x axis the Fowler - Nordheim energy and on the y axis the Fowler - Nordheim coefficient. The results of the initial measurements from Fig. 2 are displayed in circles, the green and blue circles represent the first and second measurement, respectively. The results from the illumination series are displayed in purple triangles, and the results of the temperature scan are shown in red diamonds.

In order to reduce the exposure to high voltages and powers the current limit was lowered, the measurement were stopped when the current limit was reached, and faster scan speeds were used for the irradiance series and temperature scans. Fig. 3 shows fitting results of the Fowler - Nordheim coefficient and Fowler - Nordheim energy for dark measurements at room temperature. It can be seen that there is a large difference between the first and second measurements of Fig. 2 (the blue and green circles in Fig. 3) and that differences have been greatly reduced for the irradiance series and temperature scans.

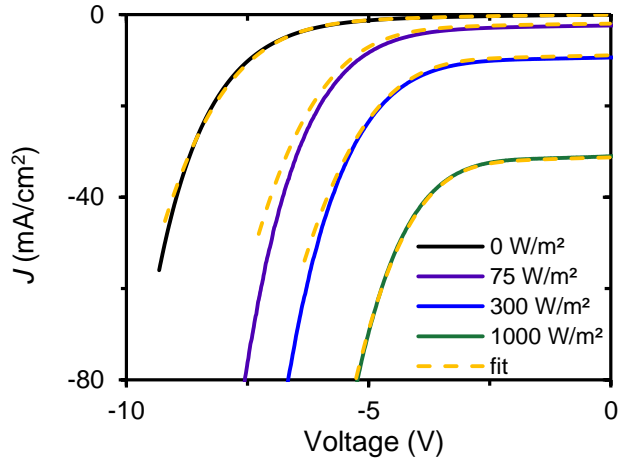


Fig. 4 Reverse JV curves at different illumination intensities. Solid curves represent the measured data and dashed curves show the fitted data.

D. Irradiance dependence

Fig. 4 shows the reverse JV curves of a number of irradiance dependent measurements from dark to 1 sun. It can be seen that the transition shifts to more negative voltages when the irradiance is decreased. This means that more energy is required in order for the solar cell to conduct the Fowler - Nordheim tunneling current. This can also be observed in the results of the fits using the SCLC and FN components, plotted in Fig. 5. In this figure a change in both FN-energy and correction factor is observed around 250 W/m^2 . This might be caused by a critical threshold for photo-conduction in the buffer layer. This behavior is in line with Puttnins *et al.* [9], who found the threshold to be around 100 W/m^2 .

With the addition of the Fowler - Nordheim correction factor this model is able to fit the light dependency of the reverse characteristic. When performing fitting to compare the different components the Fowler - Nordheim showed a better fit compared to the Poole - Frenkel in almost all cases.

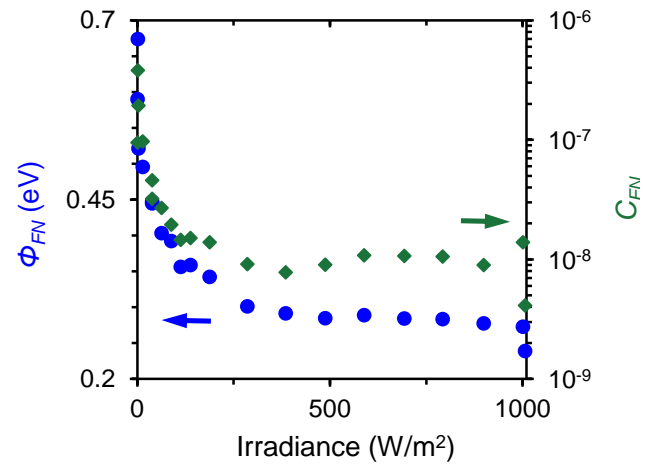


Fig. 5: Fit results (SCLC and FN) of irradiance depended reverse JV characteristics. The blue circles represent the Fowler - Nordheim energy on the left y-axis, and the green diamonds show the Fowler - Nordheim coefficient on the right y-axis.

E. Temperature dependence

Reducing the temperature will attenuate the Fowler - Nordheim tunneling current. The model is able to fit a very small FN contribution. However, fitting very low contributions is not very meaningful. Therefore the results of the dark measurements and results at temperatures below 250 K (0.004 K^{-1}) are not displayed in Fig. 6. Fig. 6 (a) shows the parameter drift at 100 W/m^2 , probably as a result of light soaking and annealing. The results of the temperature scan at 100 W/m^2 is very different compared to the scans at 300 and 1000 W/m^2 . This might be partly explained by the fact that 100 W/m^2 is in the very steep part of Fig. 5 and partly because of conditioning of the cell. During the temperature scan the cell is given time to reach a stable temperature before performing the JV scans. 100 W/m^2 is the first measurement followed by 300 and 1000 W/m^2 . In Fig. 6 (a) and (b) the results of cooling below 323 K (0.0031 K^{-1}) have been omitted. At higher illumination intensities the Fowler - Nordheim energy (Φ_{FN}) decreases linearly with temperature (Fig. 6 (b)) and the Fowler - Nordheim coefficient (C_{FN}) decreases logarithmical with temperature (Fig. 6 (c)).

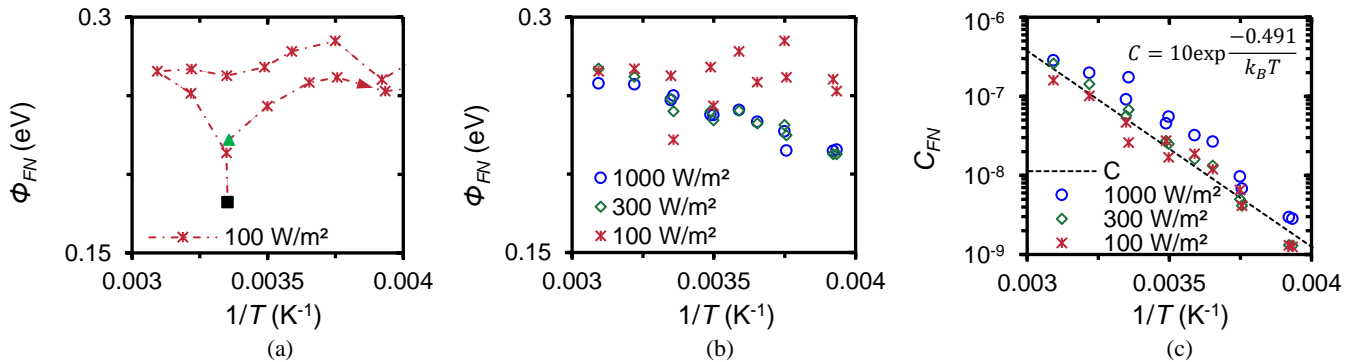


Fig. 6 Fitting results of temperature scans. (a) shows the full hysteresis of the Fowler - Nordheim energy plotted against $1/T$ at 100 W/m^2 . The measurement points are connected with a red dash dotted line with arrows indicating the scan direction. The first measurement point is indicated with a green triangle and the last measurement point is represented by a black square. In (b) and (c) the Φ_{FN} and C_{FN} are plotted against $1/T$ for illumination intensities of 100 W/m^2 (red asterix), 300 W/m^2 (green diamonds), and 1000 W/m^2 (blue circles). The black dashed line in (c) is the solution to the Arrhenius equation (equation (8)) with an activation energy of 0.491 eV.

This logarithmic decrease has an Arrhenius like behavior and follows the general Arrhenius law (8).

$$C = C_0 \exp \frac{-E_a}{k_B T} \quad (8)$$

In equation (8) C_0 is a pre-exponential factor and E_a is the activation energy. For this cell the activation energy is approximately 0.491 eV, roughly twice the Fowler - Nordheim energy.

F. Wormlike defects

The biggest challenge when studying the reverse characteristic is the formation of wormlike defects. When performing the temperature scan in the dark, even though very conservative voltage ranges were being used, several cells died. The observed temperature dependence could be partly responsible for the creation of wormlike defects. Due to local heating the reverse current will increase locally due to instantaneous heating, this increased current could lead to a critical local heating, sufficient to start the formation of wormlike defects [16], [17].

IV. CONCLUSIONS

The reverse characteristic of CIGS cells is an important, but little studied, subject. In this study a model was introduced to describe the reverse characteristic. The model consists besides the shunt resistance of two components. The space charge limited current (SCLC) is responsible for a small non-ohmic leakage current, and Fowler - Nordheim tunneling causes the sharp increase in current. In the model the Fowler - Nordheim energy (Φ_{FN}) influences the transition voltage and the Fowler - Nordheim coefficient (C_{FN}) changes the slope.

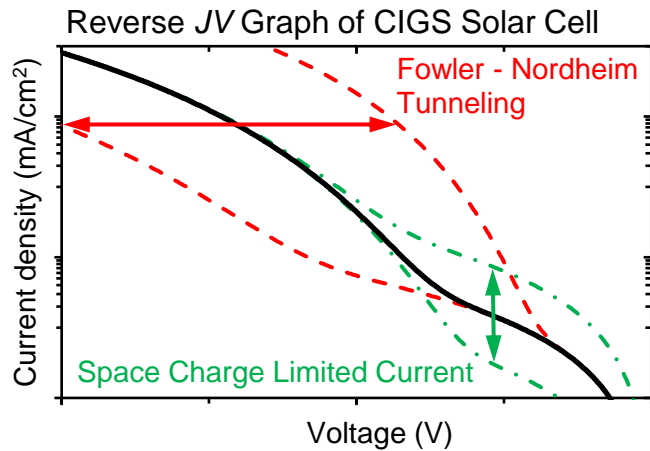
The model introduced in this study is able to describe both temperature and illumination dependency of the reverse characteristic. This would enable more accurate thermo-electrical modeling of CIGS modules under partial shading conditions. Furthermore, it would allow for more accurate studies of the reverse characteristic, as this model would allow a better description of the curve.

REFERENCES

- [1] K. Bakker, A. Weeber, and M. Theelen, "Reliability implications of partial shading on CIGS photovoltaic devices: A literature review," *J. Mater. Res.*, vol. 34, no. 24, pp. 3977–3987, Dec. 2019.
- [2] J. E. Lee *et al.*, "Investigation of damage caused by partial shading of CuInxGa_(1-x)Se₂ photovoltaic modules with bypass diodes," *Prog. Photovoltaics Res. Appl.*, vol. 24, no. 8, pp. 1035–1043, 2016.
- [3] W. Herrmann and M. C. Alonso, "Behaviour of Thin-Film Modules Under Shading," in *19th European Photovoltaic Solar Energy Conference and Exhibition*, 2004.
- [4] T. J. Silverman, L. Mansfield, I. Repins, and S. Kurtz, "Damage in Monolithic Thin-Film Photovoltaic Modules Due to Partial Shade," *IEEE J. Photovoltaics*, vol. 6, no. 5, pp. 1333–1338, Sep. 2016.
- [5] L. M. Mansfield, K. Bowers, S. Glynn, and I. L. Repins, "The Effects of Absorber Thickness on Reverse-Bias Damage in Cu(In,Ga)Se₂ Solar Cells," in *2019 IEEE 46th Photovoltaic Specialist Conference (PVSC)*, 2019.
- [6] K. Bakker, A. Rasia, S. Assen, B. Ben Said Aflouat, A. Weeber, and M. Theelen, "How the absorber thickness influences the formation of reverse bias induced defects in CIGS solar cells," *EPJ Photovoltaics*, vol. 11, no. 9, Nov. 2020.
- [7] P. Mack, T. Walter, R. Kniese, D. Hariskos, and R. Schäßler, "Reverse Bias and Reverse Currents in CIGS Thin Film Solar Cells and Modules," in *23rd European Photovoltaic Solar Energy Conference and Exhibition*, 2008, pp. 2156–2159.
- [8] P. Szaniawski, J. Lindahl, T. Törndahl, U. Zimmermann, and M. Edoff, "Light-enhanced reverse breakdown in Cu(In,Ga)Se₂ solar cells," *Thin Solid Films*, vol. 535, no. 1, pp. 326–330, May 2013.
- [9] S. Puttnins *et al.*, "Breakdown characteristics of flexible Cu(In,Ga)Se₂ solar cells," *Sol. Energy Mater. Sol. Cells*, vol. 120, no. PART B, pp. 506–511, Jan. 2014.
- [10] T. J. Silverman *et al.*, "Thermal and Electrical Effects of Partial Shade in Monolithic Thin-Film Photovoltaic Modules," *IEEE J. Photovoltaics*, vol. 5, no. 6, pp. 1742–1747, Nov. 2015.
- [11] X. Sun, J. Raguse, R. Garris, C. Deline, T. Silverman, and M. A. Alam, "A physics-based compact model for CIGS and CdTe solar cells: From voltage-dependent carrier collection to light-enhanced reverse breakdown," in *2015 IEEE 42nd Photovoltaic Specialist Conference (PVSC)*, 2015, pp. 1–6.
- [12] S. Puttnins *et al.*, "The Influence of Front Contact and Buffer Layer Properties on CIGSe Solar Cell Breakdown Characteristics," in *26th European Photovoltaic Solar Energy Conference and Exhibition*, 2011, pp. 2432–2434.
- [13] P. Szaniawski, P. Zabierowski, J. Olsson, U. Zimmermann, and M. Edoff, "Advancing the Understanding of Reverse Breakdown in Cu(In,Ga)Se₂ Solar Cells," *IEEE J. Photovoltaics*, vol. 7, no. 4, pp. 1136–1142, Jul. 2017.
- [14] S. Puttnins *et al.*, "The influence sodium on CIGSe solar cell breakdown characteristics," in *27th European Photovoltaic Solar Energy Conference and Exhibition*, 2012, pp. 2219–2221.
- [15] M. D. J. Carolus, Z. Purohit, T. Vandenbergh, M. Meuris, B. Tripathi, "Proposing an Electro-Thermal SPICE Model to Investigate the Effect of Partial Shading on CIGS PV Modules," in *35th European Photovoltaic Solar Energy Conference and Exhibition*, 2018, pp. 1343–1345.
- [16] K. Bakker, H. Nilsson Ahman, K. Aantjes, N. Barreau, A. Weeber, and M. Theelen, "Material Property Changes in Defects Caused by Reverse Bias Exposure of CIGS Solar Cells," *IEEE J. Photovoltaics*, vol. 9, no. 6, pp. 1868–1872, Nov. 2019.
- [17] K. Bakker, H. N. Åhman, T. Burgers, N. Barreau, A. Weeber, and M. Theelen, "Propagation mechanism of reverse bias induced defects in Cu(In,Ga)Se₂ solar cells," *Sol. Energy Mater. Sol. Cells*, vol. 205, p. 110249, Feb. 2020.
- [18] S. Dongaonkar *et al.*, "Universality of non-Ohmic shunt

leakage in thin-film solar cells,” *J. Appl. Phys.*, vol. 108, no. 12, p. 124509, Dec. 2010.

- [19] B. L. Williams *et al.*, “Identifying parasitic current pathways in CIGS solar cells by modelling dark J-V response,” *Prog. Photovoltaics Res. Appl.*, vol. 23, no. 11, pp. 1516–1525, Nov. 2015.
- [20] T. Walter, “Reliability Issues of CIGS-Based Thin Film Solar Cells,” in *Semiconductors and Semimetals*, 1st ed., vol. 92, Elsevier Inc., 2015, pp. 111–150.



Graphical abstract. Reverse *JV* graph of a CIGS solar cell based on the model introduced in this study. The red dashed lines show the influence of the Fowler - Nordheim mechanism on the reverse *JV* curve. The green dashed dotted lines show the influence of the Space Charge Limited Current.